Eur. Phys. J. D **44**, 17–22 (2007)
DOI: 10.1140/epjd/e2007-00158-9

THE EUROPEAN PHYSICAL JOURNAL D

The effect of an external magnetic field on the L_3 subshell fluorescence yields and level widths for Ta, W, Tl, Th and U at 59.54 keV photons

D. Demir[a] and Y. Şahin

Department of Physics, Faculty of Arts and Sciences, Ataturk University, 25240 Erzurum, Turkey

Received 15 November 2006 / Received in final form 21 February 2007
Published online 16 May 2007

Abstract. The effect of an external magnetic field on the L_3 subshell fluorescence yields (ω_3) and level widths (Γ_{L_3}) for paramagnetic Ta, W, Tl, Th and U have been investigated using the 59.54 keV incident photon energy in the external magnetic field of intensities ±0.60 T. L_3 X-ray fluorescence cross sections ($\sigma^X_{L_3}$) have been measured for the same elements. The measured ω_3, Γ_{L_3} and $\sigma^X_{L_3}$ values for $B = 0$ are in good agreement with the theoretical values. It was observed that the values of $\sigma^X_{L_3}$ and ω_3 with the applied magnitude of the magnetic field in both directions show a decreasing trend for paramagnetic Ta, W, Tl, Th and U. Furthermore, in the presence of an external magnetic field, the values of Γ_{L_3} show an increasing trend for the same elements. The results show that the atomic parameters such as spectral linewidth, radiation rates, photoionization cross section and fluorescence yield can change when the irradiation is conducted in a magnetic field.

PACS. 32.80.Hd Auger effect and inner-shell excitation or ionization – 32.80.-t Photon interactions with atoms – 32.70.-n Intensities and shapes of atomic spectral lines

1 Introduction

The primary vacancies in the L_i subshells can arise from either direct ionization by radiation, or from a shift of a K shell vacancy to the L shell. These vacancies decay through radiative, Auger and Coster-Kronig transitions. The number of L_i subshell X-rays produced per L_i subshell vacancy decay defines the subshell fluorescence yield ω_i. X-ray fluorescence parameters such as fluorescence yields and cross sections, are very important in understanding the ionization of atoms as well as for non-destructive elemental analysis in several fields such as material science, medical physics, industry and environmental science. Atomic level widths and related X-ray linewidths are of interest and value in several respects. A precise knowledge of a X-ray linewidths is very helpful to improve data analysis. Furthermore, reliable data concerning atomic level widths are important to probe the goodness of theoretical predictions concerning total vacancy lifetimes, radiative and radiationless transition probabilities, or fluorescence yields.

L X-ray fluorescence cross sections can be calculated theoretically by using photoelectric (or photoionization) cross sections, fluorescence yields, and fractional emission rates. Uncertainties in these tabulated quantities largely reflect the error in the L X-ray fluorescence cross sections. For this reason, most users prefer the experimental values of the cross sections whenever large discrepancies are observed between theoretical and experimental results. For quantitative analytical applications, it is necessary to know the different relative intensities of the photons which contribute to the fluorescence. Since fluorescence cross sections increase as the energy decrease, the contributions to the X-ray fluorescence of low-energy, low intensity transitions can be very important. Experimental L X-ray fluorescence cross sections of many elements have been measured by different groups [1–5].

Three sets of values of L_i subshell fluorescence yields ω_i and Coster-Kronig transition probabilities f_{ij} are available in the literature. The first set, complied by Krause [6], consist of the semi-empirically fitted values of ω_3 and f_{ij} for all elements in the atomic range $12 \leqslant Z \leqslant 110$. The second set of these parameters, based on the relativistic Dirac-Hartree-Slater model was tabulated by Chen et al. [7] for 25 elements in the atomic range $18 \leqslant Z \leqslant 96$. The third set of these values, Puri et al. [8] has been evaluated by using radiative and nonradiative transitions rates based on the relativistic Dirac-Hartree-Slater model all elements in the atomic range $25 \leqslant Z \leqslant 96$. In the recent years, L subshell fluorescence yields for elements were measured using radioisotopes [9–11]. Raboud et al. [12] measured L_1 to N_5 atomic level widths of thorium and uranium with transmission-type and reflection type bent

[a] e-mail: ddemir@atauni.edu.tr

crystal spectrometers. Krause and Oliver [13] presented semiemprical widths for the K and L levels. Campbell and Papp [14] assembled a rather large set of experimentally measured level widths and X-ray linewidths.

An atom in a field of electromagnetic radiation experiences interactions between its magnetic moments and the magnetic field and also between its electric charges and the electric field. The elementary electromagnetic theory explains the behavior of a magnetic dipole of moment μ_l when it is replaced in an applied magnetic field B. The dipole will experience a torque ($\vec{\tau} = \vec{\mu}_l \times \vec{B}$) tending to align the dipole with the field, and that, associated with this torque, there is a potential energy of orientation:

$$\Delta E = -\vec{\mu}_l \cdot \vec{B}. \quad (1)$$

The slight difference in energy is associated with these different orientations in the magnetic field. Thus, the atomic parameters as the shapes and the circulation properties of the electronic charge clouds, spectral linewidth, radiation rates, atomic lifetimes, photoionization cross sections and fluorescence yields can change when the irradiated atom is placed in an external magnetic field. Pavlov and Meszaros [15] investigated how the radiative transitions and the structures of the atoms in a strong magnetic field are affected.

Ionization of atoms leads to the alignment of the inner shell vacancy with the total angular momentum $J > 1/2$, where the magnetic sublevels of the resulting ion have a non-statistical population. When the irradiated atom is placed in an external magnetic field, joint action of hyperfine interaction and the magnetic field causes the alignment of the magnetic dipoles in the field direction. It is expected that the L_3 subshell fluorescence yields, level widths and photoionization cross sections can change due to the L_3 subshell vacancy states with $J = 3/2$ in the presence of an external magnetic field.

In the present work, ω_3, Γ_{L_3} and $\sigma^X_{L_3}$ for Ta, W, Tl, Th and U were measured with 59.54 keV photons in the external magnetic field of intensities ± 0.60 T. To our knowledge, L_i subshell X-ray fluorescence cross sections and L_i subshell fluorescence yields in the external magnetic field have not been reported in the literature and appear to have been measured here for the first time. The measured values for $B = 0$ were compared with theoretical results. The outline of the paper is as follows. Section 2 contains a brief description of the experimental set-up. Section 3 contains the data analysis procedure. We present, in Section 4, the measured ω_3, Γ_{L_3} and $\sigma^X_{L_3}$ values and finally our discussions and conclusions.

2 Experimental

The geometry and shielding of the experimental set-up are shown in Figure 1. Gamma photons of 59.54 keV from a filtered radioisotope ^{241}Am point source was used for direct excitation of spectroscopically pure foil of Ta and powders of W, Tl_2O_3, $Th(NO_3)_4{\cdot}5H_2O$ and $UO_2(CH_3COO){\cdot}2H_2O$. The ^{241}Am gamma source was housed at the center of

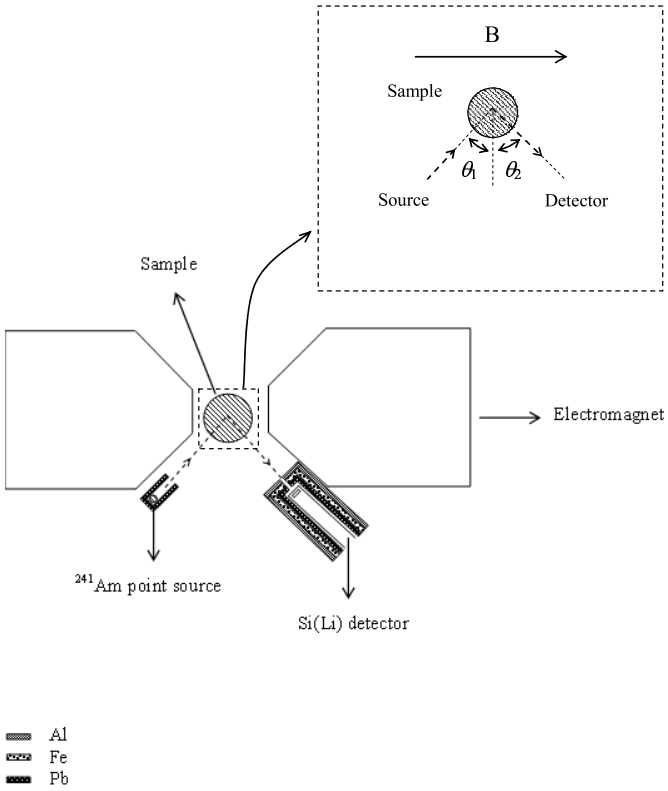

Fig. 1. Experimental set-up.

a cylindrical lead shield of 10 mm diameter and 36 mm depth. The L X-ray spectra from different samples were detected by a Si(Li) detector ($FWHM$ = 180 eV at 5.9 keV, an active diameter = 6.2 mm, sensitive crystal depth = 5 mm, Be window thickness = 0.008 mm). The detector was shielded by a graded filter of Pb, Fe and Al, to obtain a thin beam of photons scattered from the target and to prevent undesirable radiation (Np L X-rays from ^{241}Am source, L X-rays from the Pb mask, environmental background and background arising from the scattering from the sample holder and electromagnet). The data were collected into 16 384 channels of a digital spectrum analyzer DSA-1000.

The samples were mounted in a sample holder placed between the pole pieces of an electromagnet capable of producing the magnetic field of approximately 3 T at 1 mm pole range. During the study, the magnetic field intensities of ± 0.60 T were applied to the samples where + and – represent the relative directions of the magnetic field intensity. The continuity and stability of the current feeding the electromagnet were monitored by an ammeter. In order to check the systematic and the statistical counting errors arising from radiation emanating from the exciting source, a thin indium wire reference sample was positioned at the collimator of the Si(Li) detector. The accuracy of the detection system (shift and distortion of pulse-height distribution, instability and drift in instrumental components, conditions and parameters) was also checked by using the spectra of this reference sample. The

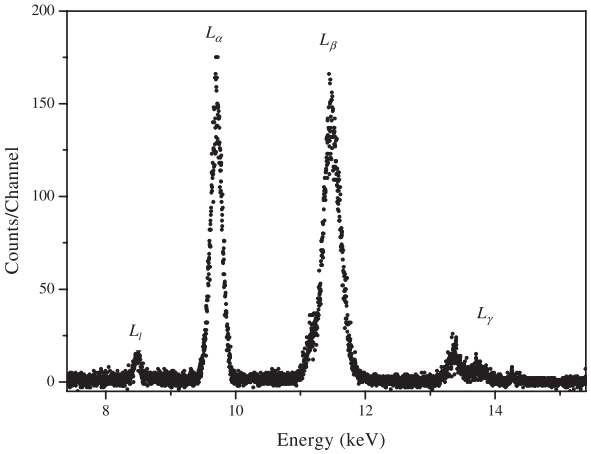

Fig. 2. A typical L X-ray spectrum of the Au target in $B = +0.60$ T.

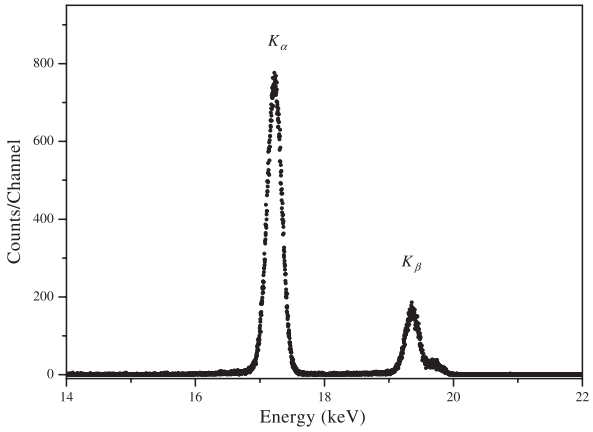

Fig. 3. A typical K X-ray spectrum of the Mo target.

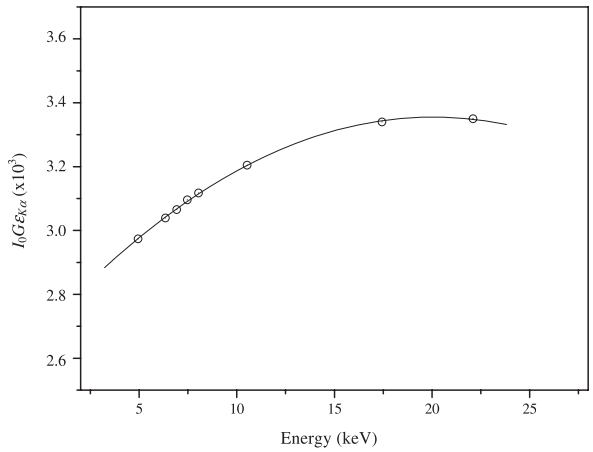

Fig. 4. The factor $I_0G\varepsilon_{K\alpha}$ as a function of a mean K X-ray energy.

pulse height spectrum of L X-rays emitted from each sample was acquired for a period of 10 h to obtain good statistics in the evaluation of each L X-ray peaks and the measurements were repeated 5 times. A typical L X-ray spectrum of Au at the $B = +0.60$ T is shown in Figure 2. The peaks due to the L_l, L_α, L_β and L_γ group of lines are well resolved. The spectra were analyzed by using Microcal Origin 7.5 Demo Version.

The counting electronics included a pile-up rejection circuit and live time clock which was used for the dead time correction. Since there is no escape peak and any other undesired effects contributing to the spectrum, the mean count of twenty channels at each side of the peaks used to calculate the background and to define the net peak area. Since the background is constant in this region a linear background function was selected to all L X-ray peaks. The background count rate was subtracted from the measurements.

3 Data analysis

The experimental L_3 subshell X-ray fluorescence cross sections have been obtained using the equation

$$\sigma_{L_\alpha} = \frac{I_{L_\alpha}}{I_0 G \varepsilon_{L_\alpha} \beta_{L_\alpha} t} \tag{2}$$

where I_{L_α} is the number of counts per unit time under the photopeak corresponding to L_α X-rays of elements, I_0 is the intensity of the exciting radiation, G is a geometrical factor dependent on the source-sample geometry, ε_{L_α} is the detector efficiency at the L_α X-ray energy, β_{L_α} is the target self-absorption correction factor for the target material, which accounts for absorption in the target of incident photons and the emitted characteristic X-rays and t is the mass per area of the element in g/cm^2.

The $I_0G\varepsilon$ values corresponding to the 59.54 keV incident photons energy were determined by measuring the K X-ray yields from spectroscopically pure targets in the atomic range $23 \leqslant Z \leqslant 47$. For these measurements the targets under investigation were replaced, in turn, with targets V, Fe, Co, Ni, Cu, As, Mo and Ag with the mass thickness 0.060–0.38 g/cm^2. A typical K X-ray spectrum of Mo is shown in Figure 3. The $I_0G\varepsilon_{K_\alpha}$ values for the present set-up were determined by the following relationship:

$$I_0 G \varepsilon_{K_\alpha} = \frac{I_{K_\alpha}}{\sigma_{K_\alpha} t \beta_{K_\alpha}} \tag{3}$$

where I_{K_α}, ε_{K_α}, β_{K_α} and t have the same meaning as in equation (2) except that they correspond to K X-rays instead of the L X-rays. The measured $I_0G\varepsilon_{K\alpha}$ values for the present geometry are plotted as a function of the mean K X-ray energy as shown in Figure 4. The theoretical values of σ_{K_α} fluorescence cross sections are calculated using the equation

$$\sigma_{K_\alpha} = \sigma_K(E)\, w_K F_{K_\alpha} \tag{4}$$

where $\sigma_K(E)$ is the K shell photoionization cross section of the given element for the excitation energy E. The values of $\sigma_K(E)$ were taken from Scofield [16] based on

Table 1. The experimental and theoretical values of $\sigma^X_{L_3}$ for Ta, W, Tl, Th and U in the external magnetic field.

Element	$\sigma^X_{L_3}$(Exp.)			$\sigma^X_{L_3}$(Theo.)
	$B = 0$	$B = +0.60$ T	$B = -0.60$ T	$B = 0$
^{73}Ta	81.89 ± 3.4	74.43 ± 3.4	74.33 ± 3.1	80.62
^{74}W	94.46 ± 4.5	85.03 ± 4.7	85.01 ± 4.3	89.70
^{81}Tl	222.44 ± 10.4	193.75 ± 11.4	192.76 ± 11.2	225.40
^{90}Th	436.77 ± 20.4	411.95 ± 19.2	412.93 ± 19.1	460.49
^{92}U	519.65 ± 31.4	454.09 ± 30.7	452.03 ± 30.2	547.83

Hartree-Slater calculations. w_K is the K shell fluorescence yield and was taken from the tables of Krause [6]. F_{K_α} is the fractional X-ray emission rate for K_α X-rays and is defined as

$$F_{K_\alpha} = \frac{I_{K_\alpha}}{(I_{K_\alpha} + I_{K_\beta})} \tag{5}$$

where $I_{K_\alpha}$and I_{K_β} are the K_α and K_β X-ray intensities, respectively. The values of I_{K_α} and I_{K_β} were taken from Scofield [17]. The self-absorption correction factor has been calculated using the following relation

$$\beta_{L_\alpha} = \frac{1 - \exp\left[-(\mu_{inc}/\cos\theta_1 + \mu_{L_\alpha}/\cos\theta_2)t\right]}{(\mu_{inc}/\cos\theta_1 + \mu_{L_\alpha}/\cos\theta_2)t} \tag{6}$$

where μ_{inc} and μ_{L_α} are the attenuation coefficients (cm^2 g^{-1}) of the incident photons and emitted characteristic X-rays, respectively, θ_1 and θ_2 are the angles of incident photon and emitted X-ray with the target. μ_{inc} and μ_{L_α} were obtained from WinXcom. This is a Windows version of XCOM [18] the well-known program for calculating X-rays attenuation coefficients.

L_3 subshell X-ray production cross section is given by the following expressions:

$$\sigma^x_{L_3} = \frac{\sigma_{L_\alpha}}{F_{3\alpha}} \tag{7}$$

where $F_{3\alpha}$ is the fraction of LX-rays originating from the L_3 transition that contribute to the L_α peak

$$F_{3\alpha} = \frac{\Gamma_{3\alpha}}{\Gamma_3} \tag{8}$$

where Γ_3 is the theoretical total radiation rate of the L_3 subshell and $\Gamma_{3\alpha}$ is the sum of the radiative transition rates, which contribute to the L_α line associated with the hole filling in the shell [17].

The experimental L_3 subshell fluorescence yields were calculated using the following expressions:

$$w_3 = \frac{\sigma^x_{L_3}}{[\sigma_3 + \sigma_2 f_{23} + \sigma_1 (f_{13} + f_{12} f_{23})]} \tag{9}$$

where σ_1, σ_2 and σ_3 were interpolated from Scofield's table [16] and f_{12}, f_{13} and f_{23} were taken from table of Krause [6].

The experimental L_3 subshell level widths were determined using following equation

$$\Gamma_{L_3} = \frac{\Gamma_{L_3}(R)}{\omega_3} \tag{10}$$

where $\Gamma_{L_3}(R)$ is the radiative transition rates of L_3 subshell.

In this work, we have calculated the theoretical L X-ray fluorescence cross sections for the elements at the 59.54 keV incident photon energy using the following equations:

$$\sigma_{L_{3l}} = [\sigma_3 + \sigma_2 f_{23} + \sigma_1 (f_{13} + f_{12} f_{23})]\, w_3 F_{3l} \tag{11}$$

$$\sigma_{L_{3\alpha}} = [\sigma_3 + \sigma_2 f_{23} + \sigma_1 (f_{13} + f_{12} f_{23})]\, w_3 F_{3\alpha} \tag{12}$$

$$\sigma_{L_{3\beta}} = [\sigma_3 + \sigma_2 f_{23} + \sigma_1 (f_{13} + f_{12} f_{23})]\, w_3 F_{3\beta} \tag{13}$$

where σ_i $(i = 1, 2, 3)$ is the L subshell photoionization cross section [16], ω_i $(i = 1, 2, 3)$ is the L subshell fluorescence yield [6], f_{ij} ($i = 1, 2$ and $j = 2, 3$) is the Coster-Kronig transition probability [6] and F_{ij} $(F_{3l}, F_{3\alpha}, F_{3\beta}, ...)$ are the fraction of the radiative transitions of the sub-shell L_i $(i = 1, 2, 3)$ contained in the jth spectral line. The F_{ij} values are given following relations

$$F_{3l} = \frac{[\Gamma (M_1 - L_3)]}{\Gamma_3} \tag{14}$$

$$F_{3\alpha} = \frac{[\Gamma (M_4 - L_3) + \Gamma (M_5 - L_3)]}{\Gamma_3} \tag{15}$$

$$F_{3\beta} = \frac{[\Gamma (N_1 - L_3) + \Gamma (N_4 - L_3) + \Gamma (N_5 - L_3)]}{\Gamma_3} + \frac{\Gamma (O_1 - L_3) + \Gamma (O_{4,5} - L_3)}{\Gamma_3} \tag{16}$$

where Γ_i $(i = 1, 2, 3)$ is total radiative width of the L_i subshell [17] and $\Gamma (X_i - Y_j)$ is the partial width. Thus, we can write following equation:

$$\sigma^x_{L_3} = \sigma_{L_{3l}} + \sigma_{L_{3\alpha}} + \sigma_{L_{3\beta}}. \tag{17}$$

4 Results and discussion

The present values of L_3 subshell X-ray fluorescence cross sections for Ta, W, Tl, Th and U at 59.54 keV incident photon energy in the external magnetic field are listed in Table 1. The overall error in the present measurements is estimated to be 4–7%. This error is the sum of the uncertainties in different parameters used to calculate the L_α X-ray production cross-sections, namely, the evaluation of peak areas ($\leqslant$2%), $I_0 G \varepsilon$ product (4–6%), target mass thickness measurements (1–2%) and the absorption correction factor ($\leqslant$2%). The errors given in Table 1 are

Table 2. The experimental values of ω_3 for Ta, W, Tl, Th and U in the external magnetic field.

	ω_3(Exp.)			Literature
Element	$B = 0$	$B = +0.60$ T	$B = -0.60$ T	Ref. [6]
^{73}Ta	0.247 ± 0.016	0.224 ± 0.015	0.223 ± 0.014	0.243
^{74}W	0.269 ± 0.017	0.242 ± 0.017	0.241 ± 0.016	0.255
^{81}Tl	0.342 ± 0.020	0.298 ± 0.019	0.297 ± 0.019	0.347
^{90}Th	0.439 ± 0.020	0.414 ± 0.020	0.414 ± 0.021	0.463
^{92}U	0.464 ± 0.029	0.405 ± 0.031	0.406 ± 0.030	0.489

Table 3. The experimental values of Γ_{L_3} for Ta, W, Tl, Th and U in the external magnetic field.

	Γ_{L_3}(Exp.)			Literature
Element	$B = 0$	$B = +0.60$ T	$B = -0.60$ T	Ref. [14]
^{73}Ta	4.708 ± 0.1	5.191 ± 0.1	5.215 ± 0.1	4.99 ± 0.31
^{74}W	4.624 ± 0.2	5.140 ± 0.2	5.162 ± 0.2	5.08 ± 0.31
^{81}Tl	5.672 ± 0.2	6.510 ± 0.1	6.532 ± 0.1	—
^{90}Th	7.362 ± 0.1	7.806 ± 0.2	7.806 ± 0.2	7.51 ± 0.1
^{92}U	7.728 ± 0.1	8.854 ± 0.2	8.832 ± 0.2	8.41 ± 0.2

estimated using the propagation of errors based on classical rules. The standard deviation of five repeated measurements obtained for Th sample is 1.04% of the arithmetic mean of these measurements. For U sample, this ratio is 0.95%. This means that the fluctuation of each measured value about the mean of each series or the statistical counting errors is small.

It is clear from Table 1 that the present experimental results for $B = 0$ are in general agreement with the theoretical values. To the best of our knowledge, no other experimental data are available for comparison with the results obtained by us for $B \neq 0$. The measured values of L_3 subshell X-ray fluorescence cross sections for the same magnitude but opposite direction of the magnetic field is almost symmetrical as seen from Table 1. This is an expected result; since there will be a tendency for the magnetic dipole moment of an atom to align about the direction of the applied magnetic field, such that the orientational potential energy is minimum. As seen from Table 1, the values of L_3 subshell X-ray fluorescence cross sections for paramagnetic samples show a decreasing trend with the applied magnitude of the magnetic field in both directions. The magnetic field dependency of L_3 subshell X-ray fluorescence cross sections can be explained with the interaction of magnetic dipole moment with the external magnetic field.

The values of L_3 subshell fluorescence yields (w_3) decided using equation (9), for same elements are presented in Table 2. The semiempirical values of Krause [6] are also given in Table 2. It is clear from Table 2 that the present experimental values for $B = 0$ are in general agreement with the values of Krause for all elements. Since experimental results L_3 subshell fluorescence yield for $B \neq 0$ cannot be found in the literature, the comparison is not made with the other experimental values. It is clear from Table 2 that the investigated L_3 subshell fluorescence yields are symmetrical as expected for the same magnitude but opposite direction of the magnetic field.

In Table 3, the present level widths of L_3 are compared with Campbell and Papp [14]. For $B = 0$, the present results are different than 1–8% for values of Campbell and Papp [14]. As seen from Table 3, the values of level widths L_3 with the applied magnitude of the magnetic field in both directions show an increasing trend for paramagnetic samples. The results show that the transition probabilities L_α lines show a decreasing trend for paramagnetic samples in the external magnetic field. This result probably arises from the alignment of the vacancy states with $J > 1/2$ with external magnetic field.

In the ionization of an inner atomic electron by radiation, the ionized target atom turns out to be aligned in the direction of the incident beam. When the irradiated atom is placed in an external magnetic field, joint action of hyperfine interaction and the magnetic field causes the alignment of the magnetic dipoles in the field direction. Thus, both the radiation field and an external magnetic field lead to the alignment of the inner shell vacancy in ions. The concepts of alignment and orientation can be defined for the general case of an excited state having arbitrary angular momentum. The vacancy states with $J = 1/2$, K shell and L_1 and L_2 subshell, created by the direct photoionization of atomic inner shells by unpolarized radiation, exhibit isotropic spatial distributions as their magnetic sublevels with $M_J = \pm 1/2$ are equally populated. The decay of these vacancy states results in an isotropic emission of X-rays. Thus, the L_3 subshell vacancy states with $J = 3/2$ will be aligned and their decay will result in an anisotropic emission L subshell X-rays.

In conclusion, the magnetic field dependency of L_3 subshell X-rays clearly establish that the atomic parameters such as the shapes and the circulation properties of the electronic charge clouds, spectral linewidth, radiation rates, photoionization cross sections and fluorescence yields can change in an external magnetic field. According to the results presented here, it is possible to enhance the anisotropic emission of L_3 X-rays with an external magnetic field. The best of our knowledge there are no reports regarding effect of an external magnetic field to the ω_3, $\Gamma_{L_3}$and $\sigma^X_{L_3}$ for Ta, W, Tl, Th and U. To obtain more definite conclusions on the magnetic field dependency of

the atomic parameters, more experimental data are clearly needed, particularly in the heavy elements region.

References

1. M. Şahin, L. Demir, Ö. Söğüt, M. Ertuğrul, O. İçelli, J. Phys. B: At. Mol. Opt. Phys. **33**, 93 (2000)
2. R.R. Garg, S. Puri, S. Singh, D. Mehta, J.S. Shahi, M.L. Garg, N. Singh, P.C. Mangal, P.N. Trehan, Nucl. Instr. and Meth. B **72**, 147 (1992)
3. M. Ertuğrul, J. Radioanal, Nucl. Chem. **237**, 139 (1998)
4. A.C. Mandal, S. Santra, D. Mitra, M. Sarkar, D. Bhattacharya, Nucl. Instr. Meth. B **234**, 176 (2005)
5. K.A. Al-Saleh, N.S. Saleh, Radiat. Phys. Chem. **54**, 117 (1999)
6. M.O. Krause, J. Phys. Chem. Ref. Data **8**, 307 (1979)
7. M.H. Chen, B. Crasemann, H. Mark, Phys. Rev. A **2**, 177 (1981)
8. S. Puri, D. Mehta, B. Chand, P.N. Trehan, X-Ray Spectrom. **22**, 358 (1993)
9. A. Rani, N. Nath, S.N. Chaturvedi, X-Ray Spectrom. **18**, 7780 (1989)
10. E.V. Bonzi, N.M. Badiger, Nucl. Instr. Meth. B **248**, 242 (2006)
11. R. Durak, Y. Özdemir, J. Anal. At. Spectrom. **16**, 1167 (2001)
12. P.A. Raboud, J.L. Dousse, J. Hoszowska, I. Savoy, Phys. Rev. A **61**, 1 (1999)
13. M.O. Krause, J.H. Oliver, J. Phys. Chem. Ref. Data **8**, 328 (1979)
14. J.L. Campell, T. Papp, At. Nucl. Data Tables **77**, 1 (2001)
15. G.G. Pavlov, P. Meszaros, Astrophys. J. **416**, 752 (1993)
16. J.H. Scofield, UCRL Report 51326 Lawrence Livermore Laboratory CA (1973)
17. J.H. Scofield, At. Nucl. Data Tables **14**, 121 (1974)
18. L. Gerward, N. Guilbert, K. Bjorn, H. Levring, Radiat. Phys. Chem. **60**, 23 (2001)